Colloids and Surfaces B: Biointerfaces 178 (2019) 66–73

Contents lists available at ScienceDirect

Colloids and Surfaces B: Biointerfaces

journal homepage: www.elsevier.com/locate/colsurfb

Protocols

Additive-based stability assessment of biologically designed CuO and GSH-CuO nanospheres and their applicability as Nano-biosensors

Noor-ul Ain, Naila Safdar*, Azra Yasmin

Microbiology and Biotechnology Research Lab, Department of Biotechnology, Fatima Jinnah Women University. Pakistan Old Presidency, the Mall, Rawalpindi, 46000, Pakistan

ARTICLE INFO

Keywords:
CuO nanoparticle
Biosensor
Peroxidase mimics
Nanozymes
Glutathione

ABSTRACT

Uncapped and Glutathione capped Cupric oxide nanospheres were synthesized by the interaction of *Berberis lycium* (Bl) root extract with corresponding salt solution. CuO nanospheres were best optimized by mixing 2% Bl extract solution with 1 mM $CuSO_4{\cdot}5H_2O$ (pH 11, 90 °C) Reduced glutathione (0.25 mM) in solution form was added in respective emulsion after 24 h. Synthesis of nanospheres was ensured by distinct surface plasmonic resonance peaks shown by CuO (370–420 nm). Addition of glutathione resulted in sharp blue shift and lowered absorbance values in UV spectra suggesting the decrease in nanoparticles' size and concentration. Average particle sizes as deduced with XRD were found to be 18.52 and 16.57 nm for CuO and GSH-CuO nanospheres respectively. Additive based stability assessment of synthesized nanospheres revealed CuO and GSH-CuO nanospheres to be highly stable in the presence of Catechin hydrate among various tested chemical compounds while ascorbic acid appeared as a strong destabilizing agent. TMB was oxidized by H_2O_2 in the presence of synthesized enzymes likewise horseradish peroxidase; though exhibited moderate results. Glutathione stabilized cupric oxide nanospheres exhibited the potential to be modulated further into efficient nanozymes as these showed better affinity towards chromogenic substrate TMB (K_m value 0.32 mM) and better catalytic efficiency (0.075 $mM^{-1}\,s^{-1}$) compared to uncapped CuO nanomimetics (1.6 mM, 0.033 $mM^{-1}\,s^{-1}$). All of the tested additives served as inhibitors to the peroxidase mimicking potential of CuO and GSH-CuO nanozymes.

1. Introduction

Phytonanotechnology is getting an edge over usual physiochemical approaches because of ease of manipulation, cost effectiveness and environmentally benign nature. Biomolecular profile of plants has a significant impact on their metal ion reducing capability. Various effective biomolecules which are involved in the process include proteins, amino acids, alkaloids, polysaccharides and chelating agents etc. Metal ions after binding with plant metabolites and stabilizing agents get reduced to atoms which on interacting with similar complexes result in the formation of metal nanoparticles [1].

Copper oxide nanoparticles have been prepared by various methods (chemical, physical, biological) and found valuable in numerous applications as reported in existing literature. For instance, CuO synthesized from plant sources have been reported as potent antimicrobials [2], highly cytotoxic against tested cancer cell lines [3] as well as cost-effective dye-degraders as observed in case methylene blue [4]. The catalytic potential of biologically synthesized CuO nanoparticles and their composites is also well-established in literature [5–7]. Various biomolecules such as nucleic acid, oligonucleotides, peptides and antibodies have been used for capping of novel metal nanoparticles in order to impart these improved characteristics such as enhanced stability or functionality [8]. Among such modulators, Glutathione; a naturally occurring tripeptide biomolecule has been utilized for capping of various nanoparticles with successful outcomes [9]. Since metals exhibit high affinity for thiol group, the functionalization of nanoparticles by glutathione has proven to be beneficial in case of metallic and bimetallic nanoparticles' formulation [10].

Nanozymes have demonstrated individuality in terms of their increased stability, robustness, reusability, cost effectiveness, integrated multi-functions besides catalysis, large surface area for further modification and better response to external stimuli [11]. Given a huge spectrum of applications offered by natural peroxidases, peroxidase mimicking nanozymes have gained much importance since natural

Abbreviations: SPR, surface plasmonic resonance; TMB, 3,3′,5,5′-tetramethylbenzidine; GSH, reduced glutathione; HRP, horseradish peroxidase; Bl, *Berberis lycium*; K_m, Michaelis menten constant; K_{cat}, catalytic constant

* Corresponding author.
E-mail addresses: noorain20.na@gmail.com (N.-u. Ain), nailahussain@fjwu.edu.pk (N. Safdar), azrayasmin@fjwu.edu.pk (A. Yasmin).

https://doi.org/10.1016/j.colsurfb.2019.02.048
Received 3 October 2018; Received in revised form 22 February 2019; Accepted 22 February 2019
Available online 23 February 2019
0927-7765/

peroxidases suffer from the problematic issues of purification and isolation steps resulting in their denaturation [12]. The utilization of Horseradish peroxidase in H_2O_2 bio-sensing has long been established given the enzyme's ability to oxidize number of substrates in the presence of H_2O_2. Usually, HRP is immobilized over a suitable mediator which enables efficient electron transfer between HRP and the substrate in a more effective manner. This increases the sensitivity of the biosensor while lowering the detection limit to a much greater extent [13]. In present era, researchers are focusing their attention towards the formulation of nanomaterials which could mimic HRP in best possible manner and could come forward as efficient Nano-biosensors. Wide range of POx mimicking nanozymes have been synthesized and tested for their sensing potentialities for H_2O_2 and other biomolecules [14–16]. Until now, majority of the work regarding peroxidase mimicking Nano biosensors is based upon chemically synthesized nanostructures [17–19].

However, given the utilization of chemicals as reducing agents, these methods may lead to the primary issues of environmental toxicity and greater expense. Thus in order to overcome such problematic issues, CuO nanoparticles were synthesized using *Berberis lycium* root extract under optimum conditions. Bl roots were used as reducing agent due to the established medicinal importance of the plant for treatment of various disorders and this immense usefulness of Bl roots is attributed to its rich phyto-chemical profile [20]. Both capped and uncapped CuO nanostructures were then characterized and subjected to stability test in the presence of selective bio-medically significant compounds followed by Steady-State Kinetic assays. This would help in determining the intrinsic peroxidase potential of synthesized nanostructures as a potential Nano-biosensor alternative to existing options.

2. Material and methods

2.1. Sample collection

Fresh roots of *Berberis lycium* Royle were collected from its natural habitat (Northern areas of Pakistan). The roots were thoroughly washed, shade-dried and then ground into fine powder for preparation of aqueous extract as reported in our previous study with minor modifications [21].

2.2. Synthesis and functionalization of copper oxide nanoparticles

Equal volumes of 1 mM $CuSO_4{\cdot}5H_2O$ and 2% *Berberis lycium* root extract prepared separately in double distilled water were combined and pre-warmed up to moderate temperature before mixing together (pH = 11). The solution was shaken vigorously for 1 h and then kept under incubation at 90 °C ± 2 for 72 h. The darkening of solution indicated the presence of dark brown CuO nanoparticles in the form of precipitates. The solution was centrifuged (15 min, 3500 rpm) and washed at least twice with ddH_2O for complete removal of impurities. The supernatant was discarded while the remaining pellets were air-dried and stored in the form of fine particles. The performed protocol was in unison with that reported by [22] with certain required modifications. For capping of CuO NPs, different concentrations of glutathione and incubation time/temperature with the selected salt solution were optimized. After optimization, the nanoparticle emulsion was interacted with 0.25 mM GSH concentration (pH = 11, temp = 90 °C) under vigorous stirring for 30 min following incubation of emulsion for another 24 h.

2.3. Characterization of CuO/GSH-CuO nanoparticles

The UV–vis spectra of the emulsions was monitored with the help of Shimadzu U.V 1602. Biotechnology medical services (BMS) within the range of 300–700 nm with resolution of 1 nm and scanning speed of 300 nm/min. FTIR analysis of manufactured nanoparticles and crude plant extract was performed via

Shimadzu FTIR 8400. The equipment used for X-Ray diffraction analysis was X-ert Pro (Banalytical) analytical X-Ray diffractometer [40 kV, 30 mA]. For visualization of surface topography and determination of individual sizes of prepared nanoparticles, samples were subjected to Scanning Electron Microscope using Ion Sputtering Device JFC-1500 [5,000–50,000X, 10–20 kV].

2.4. Stability assessment of CuO/GSH-CuO nanoparticles

Both types of prepared nanoparticles were evaluated for their stability in the presence of biologically significant compounds i.e. EDTA-disodium, Ascorbic acid, Catechin hydrate, Phenol, Mercuric chloride and Lead nitrate. 0.5 mM of each compound was added individually in the prepared nanoparticles' emulsions (incubated at 90 °C) and the effects of their incorporation were monitored by observing UV–vis absorbance spectra at intervals of 1, 6 and 24 h time period. Nanoparticles' stability was evaluated with the help of UV–vis absorbance peak intensities (%) determined by comparison of control and modulated samples [23].

2.5. Enzyme kinetics of CuO/GSH-CuO nanoparticles

Steady State Kinetics of CuO/GSH-CuO nanoparticles were studied by preparing reaction mixtures with 1700 µl of Phosphate Buffer Saline (0.1 M, pH 5), 100 µl of CuO/GSH-CuO NPs (100 µg/ml prepared in PBS) and varying concentrations of TMB (0.5, 1, 1.5, 2, 2.5, 3, 3.5, 4 mM) with fixed H_2O_2 concentration i.e. 100 mM Absorbance data was collected at 652 nm with 30 s gap for 4 min. Initial velocities (V_o) in µMol/min were then calculated by substituting absorbance data into Beer-Lambert law, and plotted as a function of substrate concentrations in Michaelis-Menten curve in order to determine V_{max} (maximum initial velocity obtained at specific substrate concentration) and K_m (the substrate concentration at which V_{max} is half of its value) using Lineweaver Burk Plot [24]. Steady-State Kinetics was studied for commercial HRP in order to compare the binding affinities of natural enzyme and synthesized nanoparticles. The catalytic efficiency was also calculated for each enzymatic entity in order to determine the overall capability of a catalyst to convert substrate into product.

2.6. Evaluation of enhancers/inhibitors' effect on POx activity of native HRP and CuO/GSH-CuO nanoparticles

The aforementioned chemical compounds utilized for stability assessment of synthesized nanoparticles were also tested for their influence upon catalytic efficacy of prepared nanoparticles [25]. Known concentration of each compound was added into the solution containing 10 µl of HRP/CuO/GSH-CuO NP, TMB (2 mM), H_2O_2 (100 mM) and 1700 µl of PBS (0.1 M, pH 5). The effect of all additives on the oxidation rate of TMB by each catalytic entity was monitored by means of plotting absorbance vs time graph by measuring absorbance after every 30 s for 4 min.

3. Results

3.1. Identification and characterization of nanoparticles

The reduction of salt precursor i.e. $CuSO_4.5H_2O$ into CuO nanostructures was visually observed through color change of reaction mixture during ionic to atomic state conversion. UV–vis Spectrophotometry was performed in order to analyze the position of SPR peak at specific wavelength characteristic to CuO nanospheres. The absorbance spectra was monitored under the 300–700 nm range since CuO nanoparticles exhibited maximum UV-absorbance between 370–425 nm wavelengths depending upon varying pH (7, 9, 11) and precursor salt concentrations (0.5, 1, 2 mM). Since the maximum absorbance of SPR peak (at 425 nm)

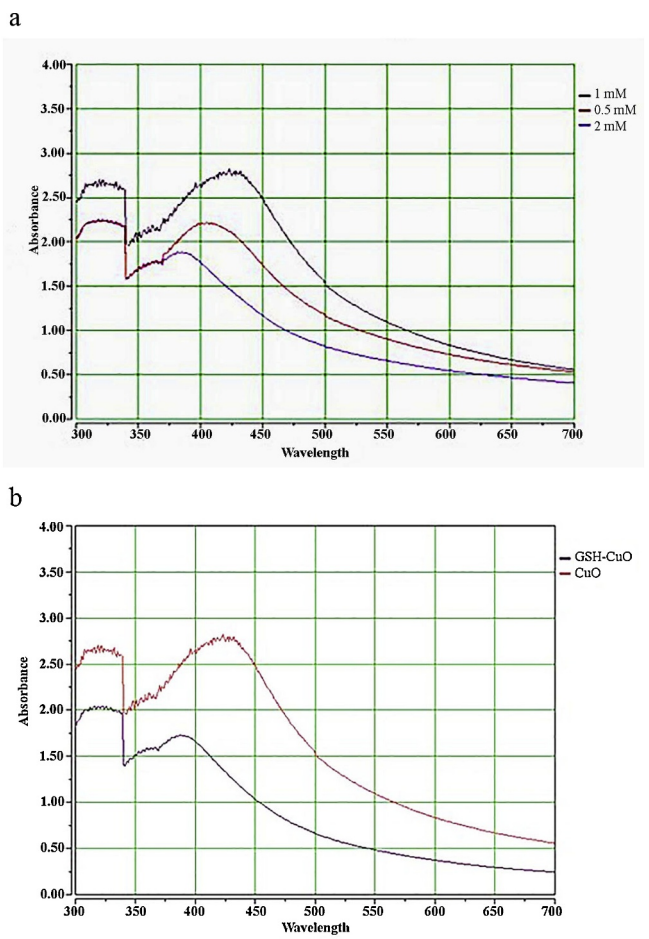

Fig. 1. Absorbance spectra of CuO NPs at pH 11 with varying $CuSO_4.5H_2O$ concentrations (a) followed by their capped and uncapped synthesis (b).

was noted at pH 11 and 1 mM $CuSO_4.5H_2O$ concentration, the aforementioned conditions were selected for subsequent synthesis of CuO nanoparticles (Fig. 1a). Upon the addition of reduced glutathione to encapsulate synthesized CuO nanoparticles, the absorption spectrum showed notable decrease in absorbance along with the blue shifting of peak from 425 to 385 nm under similar conditions (Fig. 1b). The difference in two absorbance spectra was mainly due to the attachment of glutathione with nanoparticles causing a shift in SPR of CuO nanoparticles.

FTIR analysis of original and modified CuO nanoparticles was performed and compared with that of *Berberis lycium* root extract in order to validate the involvement of various phyto-constituents in nanoparticles' formulation (Fig. 2). The spectral bands at 1560.46 cm^{-1} (N−H bend of secondary amine), 1654.9 cm^{-1} (C=C stretch of vinyledene compound), 2852.81 cm^{-1} (C–H, O−H and N−H stretch of alkane, alcohol and amine salt respectively) and 2225.93 cm^{-1} (C≡N stretch of nitrile) found in curve A of Bl extract were completely utilized in curve B signifying IR spectrum of CuO nanoparticles. The strong bands at 707.90 cm^{-1} (C=C bend of alkene), 947.08 cm^{-1}(O−H bend of carboxylic acids), 1465.95 cm^{-1}(C–H bend of alkane) and 1741.78 cm^{-1} (C=O stretch of ester) found in curve B (CuO NPs) were completely utilized in curve C (GSH-CuO NPs). Several others bands found in plant extract showed shifting and change in peak intensities of GSH-capped and uncapped nanoparticles. XRD analysis of prepared structures i.e. CuO and GSH-CuO nanospheres exhibited diffraction peaks which were confirmatory to a monoclinic crystalline structure. The most prominent peaks were observed around 2θ values between 35°- 40° with minute deviation in case of uncapped and GSH-capped structure (Fig. 3a, b). The average crystallite sizes determined with the help of Debye-Sherrer's equation were found as 18.52 nm and 16.57 nm for CuO and GSH-CuO NPs respectively. The dislocation density calculated as [26] was found equal to 29.15×10^{-4} $(nm)^{-2}$ and 36.42×10^{-4} $(nm)^{-2}$ for CuO and GSH-CuO nanospheres respectively.

The typical SEM imagery of CuO and GSH-CuO NPs can be seen in Fig. 4(a, b). Scanning electron microscope revealed nanoparticles to be spherical particles with rather rough surface topography. In unison to the crystallite size obtained by XRD, the minimum particle size observed for GSH-CuO NPs was found relatively smaller than that of unmodified CuO NPs i.e. 20 nm for GSH-CuO and 24 nm in case of CuO nanospheres.

3.2. Influence of various additives on CuO and GSH-CuO nanoparticles' stability

The stability of original and glutathione capped CuO nanospheres was evaluated in the presence of various additives i.e. $HgCl_2$, Phenol, EDTA, Catechin hydrate, Pb $(NO_3)_2$ and Ascorbic acid owing to their biomedical significance. Aforementioned additives when interacted with synthesized nanoparticles, resulted in absorbance changes and wavelength shifts of UV–vis spectra of control samples. Absorbance peak retention in the presence of each additive was calculated from the following formula:

Peak retention (%) = (Peak absorbance of tested sample/ Peak absorbance of control) × 100 (2)

Among various compounds, Catechin hydrate revealed best compatibility with synthesis of CuO/GSH-CuO nanostructures, in the presence of which absorbance peaks were found increased than their control counterparts. On the other hand, Ascorbic acid was found as least compatible to the synthesized nanoparticles among various additives that were examined (Table 1). Stability assessment of synthesized nanostructures in the presence of tested chemicals showed following trend in terms of highest to lowest compatibility levels in case of CuO (3) and GSH-CuO (4) nanospheres.

Catechin hydrate > Phenol > $HgCl_2$ > EDTA > Pb $(NO_{3)2}$ > Ascorbic acid (3)

Catechin hydrate > $HgCl_2$ > Phenol > Pb $(NO_3)_2$ > EDTA > Ascorbic acid (4)

3.3. Steady state kinetics of HRP and synthesized CuO/GSH-CuO nanospheres

The reaction mixtures containing phosphate buffer saline (0.1 M, pH: 4.5), H_2O_2, TMB and natural/synthetic enzymatic entity were prepared at room temperature and the kinetics were studied at 652 nm using UV–vis spectroscopy relative to oxidized TMB which leads to the rapid change in color of reaction mixture from transparent to bright blue (Fig. A1). The concentration of catalytic entity was opted after observing the intensity of color change of reaction mixture. This required the use of twice the concentration of enzyme mimicking nanoparticles compared to HRP concentration used in reaction.

In order to determine the peroxidase mimicking efficiency of synthesized CuO and GSH CuO NPs, both types were subjected to steady state kinetics in order to analyze their binding affinity for the peroxidase substrate i.e. TMB. The Michaelis Menten curves and Lineweaver Burk Plots obtained for both types of NPs can be observed in Figs. A2 and A3. The K_m and V_{max} values were obtained for each sample and compared with that obtained for commercial HRP. Table 2 highlights the K_m and V_{max} values obtained for HRP, CuO and GSH-CuO through steady state kinetics assay. Among all catalytic entities under study, the K_m value was found minimum in case of Glutathione capped CuO nanospheres (100 μg/ml). Different concentrations of native horseradish peroxidase (50 μg/ml) and peroxidase mimetics (100 μg/ml) were

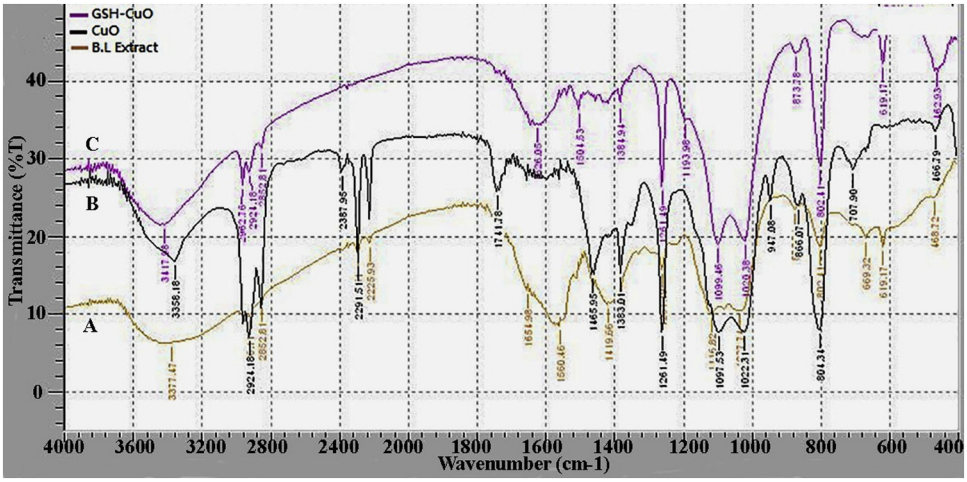

Fig. 2. FTIR spectra of (i) Bl Extract (curve A) (ii) CuO NPs (curve B) and (iii) GSH-CuO NPs (curve C).

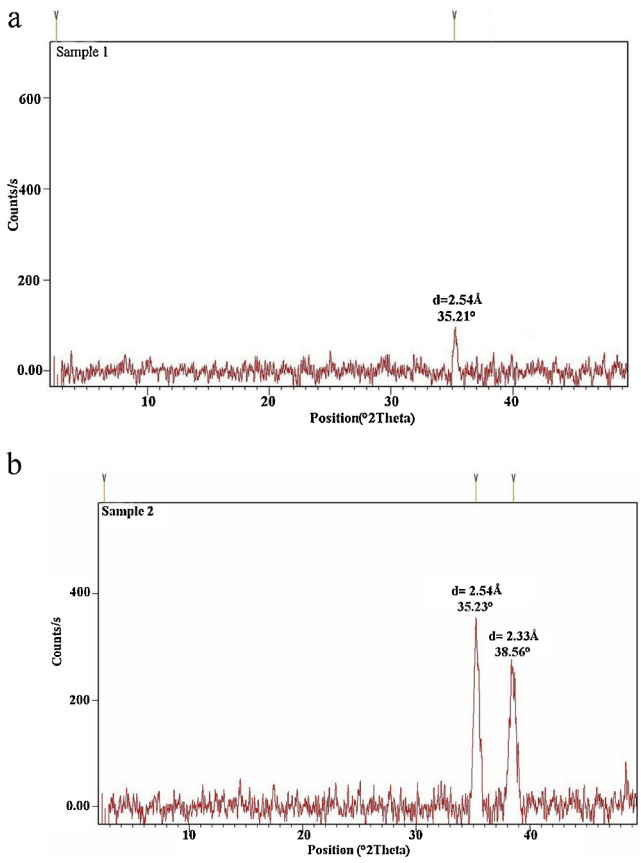

Fig. 3. (a, b): XRD pattern of uncapped (sample 1) and capped CuO nanospheres (sample 2).

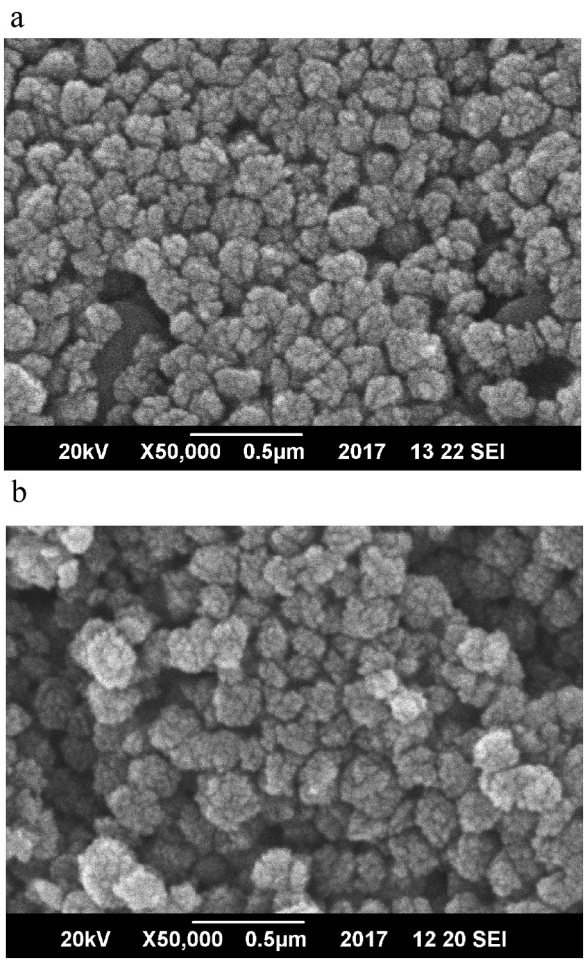

Fig. 4. (a, b): SEM imagery of (a) uncapped CuO nanospheres and (b) GSH-CuO nanospheres.

utilized for proceeding the TMB-H_2O_2 reaction given the indiscernible oxidation capability shown by CuO and GSH-CuO enzyme mimics at lower concentration. Catalytic efficiency of HRP was found highest whereby among the uncapped and capped CuO nanospheres, increased catalytic efficiency was calculated in case of GSH-capped CuO nanospheres (Table 2).

3.4. Influence of additives on POx activity of native HRP, CuO and GSH-CuO nanospheres

In order to determine the enhancing or inhibiting effect of already stated bio-medically important chemical compounds upon the POx activity of natural enzyme and enzyme mimetics, only those compounds were selected in the presence of which formulated nanoparticles were found relatively stable i.e. Catechin hydrate, Phenol, $HgCl_2$ and $Pb(NO_3)_2$. Fig. 5(a–c) illustrates the time-dependent absorbance spectra of HRP and CuO/GSH-CuO nanospheres in the presence of selected compounds. TMB oxidation rate in case of HRP was found increased in the presence of lead nitrate compared to that of standard

Table 1
Additive based stability assessment observed for CuO/GSH-CuO nanospheres.

No.	Chemical Compound / Incubation time	Peak retention %					
		CuO	GSH-CuO	CuO	GSH-CuO	CuO	GSH-CuO
		1 hour		6 hours		24 hours	
1.	Mercuric chloride	96.9	92.3	96.8	92.8	99.1	92.5
2.	Catechin hydrate	101	105	101	105.7	104	105.5
3.	Phenol	95.08	94.3	94.9	106.6	99.3	98
4.	Lead nitrate	102.5	54.9	99.4	29.1	82.2	46.5
5.	Ascorbic acid	48.65	3.6	46.9	3.6	42	3.6
6.	EDTA	62.64	70	61	66.98	65.6	61.1

reaction mixture. Although $HgCl_2$, Catechin hydrate and Phenol led to the reduction in TMB oxidation rate however, $HgCl_2$ exhibited maximum quenching effect upon the reaction in case of CuO and GSH-CuO nanozymes. Meanwhile, reaction system utilizing CuO nanospheres as enzyme mimic showed least quenching effect by Phenol whereas in case of GSH capped CuO nanospheres, Catechin hydrate was found most compatible with the TMB oxidation reaction. Overall, all the tested additives appeared to act potentially as inhibitors to the enzymatic activity of synthesized nanozymes.

4. Discussion

4.1. Nanoparticle characterization by UV–vis spectroscopy

Copper oxide nanoparticles, in the current study, exhibited prominent UV-absorbance peak within 380–420 nm wavelength range (Fig. 1). The results obtained revealed that at both the concentrations of $CuSO_4.5H_2O$ i.e. 0.5 and 1 mM, greater concentration of larger sized nanoparticles was obtained at higher pH values i.e. 9 and 11 while relatively smaller nanoparticles in lower concentration were formed at pH 7. It has been established in previous literature that blue shift in peak wavelength occurs due to small sized nanoparticles while red shift of absorption spectrum marks the presence of larger nanoparticles. Moreover, the aggregation of nanoparticles mainly results in the broadening and shifting of peaks to longer wavelengths [27]. High pH value has been found critical in the synthesis of CuO nanoparticles since at lower pH, there is a high possibility that the solution contains a mixed ratio of Cu_2O and CuO nanoparticles [28]. During phytosynthesis of nanoparticles, pH variation causes change in the charge of natural phytochemicals, which in turn impacts upon their binding capability and the reduction of metal ions thereby affecting the morphology and yield of synthesized nanoparticles [29]. In the present scenario, higher pH facilitated plant extract in playing its reduction role more effectively and pH 11 was finalized for the synthesis of CuO nanoparticles for further manipulation. Since both types of capped and uncapped nanoparticles were synthesized at elevated temperature, the most acceptable nanoparticle growth mechanism that can be suggested in this case is Ostwald ripening and aggregation of nanoparticles aided by high Brownian coagulation rate. Firstly, coarsening of particles took place where large particles were formed by grouping of smaller particles and then aggregation occurred because of increased particle mobility and coalescence. Thus, primary nanoparticles might have resulted in the formation of large nanocrystals [30].

4.2. Mechanism of CuO nanospheres synthesis

Number of researchers have agreed upon the fact that phytochemical constituents mainly phenolics, flavones, terpenoids, alcohols, polysaccharides and many other play a major role in the reduction of metal salts. The mechanism involved in the synthesis of CuO nanoparticles is quite straightforward. According to our assumption, firstly $CuSO_4.5H_2O$ was reduced into Cu $(OH)_2$ by reacting with hydroxyl ion generated by water. Secondly, Cu $(OH)_2$ was further reduced into CuO nanostructures by active phyto-constituents occurring in Bl extract. Following reactions proposes the pathway involved in CuO nanoparticles formulation.

$$CuSO_4{\cdot}5H_2O + 2OH^- \rightarrow Cu\ (OH)_2 + {SO_4}^{2-} + 5H_2O$$

$$Cu\ (OH)_2 + [\text{Phytochemicals in Bl extract}] \rightarrow \text{CuO NPs} + H_2O$$

4.3. Finding from FTIR and XRD analysis

The FTIR spectrum of Bl root extract revealed the presence of numerous functional group which attributed to the presence of proteins, alkanes, phenols and alcohols, flavonoids, alkyl halides and aromatic compounds. Many of the peaks indicating the presence of above mentioned compounds were found unaltered with a negligible shift in frequencies in the IR spectrum of CuO NPs mainly 1097.53 cm^{-1}, 1261.49 cm^{-1} (both indicating C–O group) and 2924.18 cm^{-1} (indicating C–H, N—H and O—H groups) which led to the assumption that associated compounds served as capping agents encapsulating the

Table 2
Kinetic parameters of Native HRP and Peroxidase mimics.

Enzyme utilized (temp: 30 °C)	Substrate	Enzyme Conc. (μg/ml)	Michaelis Menten constant K_m (mM)	Maximum Velocity V_{max} (μM/min)	Catalytic constant k_{cat} (s^{-1})	Catalytic efficiency ($mM^{-1}\,s^{-1}$)
Horseradish Peroxidase	TMB (varying), H_2O_2 (fixed)	50	2.1	3.8	0.76	0.36
CuO nanoparticles		100	1.6	5.3	0.053	0.033
GSH-CuO nanoparticles		100	0.32	2.4	0.024	0.075

Kcat = $V_{max}/[E]_o$ (Here, V_{max} = maximum reaction velocity, $[E]_o$ = total enzyme concentration used in the reaction, Catalytic efficiency = k_{cat}/K_m.

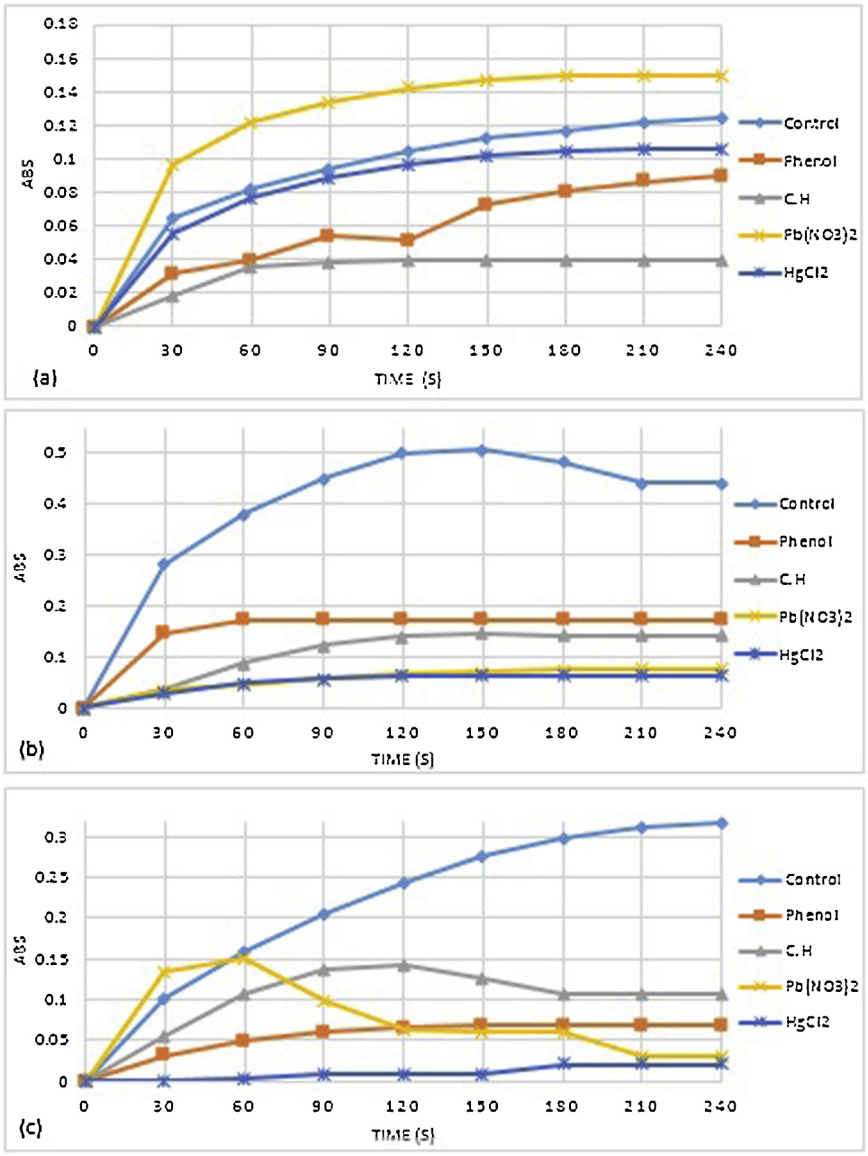

Fig. 5. Time-dependent absorbance spectra of TMB oxidation (652 nm) in the presence of additives by (a) native HRP (b) CuO nanospheres and (c) GSH-CuO nanospheres.

exterior of nanoparticles. On the other hand, some bands such as 1037.74 cm^{-1}(proteins) and 1654.98 cm^{-1} (flavonoids) were totally consumed during CuO NPs synthesis. Meanwhile, peaks observed within the range of 600–1050 cm^{-1} in FTIR analyses of capped and uncapped nanostructures could also be attributed to metal-oxide stretching of Cu—O as suggested previously [29]. A slight variation was observed among the IR spectra of uncapped and GSH capped CuO nanospheres with minor shifts in bands which might have occurred due to the interference of glutathione capping the nanoparticles (Fig. 2).

The XRD patterns of both CuO and GSH-CuO nanostructures were found confirmatory to the monoclinic crystalline structure. The average crystallite size calculated in both cases revealed smaller average size in case of capped CuO nanoparticles. This might have resulted due to the effective stabilization role played by Glutathione. Reduced glutathione (GSH), a composite of L-glutamine, L-cysteine and glycine, has been used previously for capping of nanoparticles as its functional groups −SH, −COOH and $-NH_2$ exhibit high affinity towards metal ions and result in the synthesis of highly stable, non-toxic nanoparticles with favorable properties [9]. However, it must be noticed that average crystallite size of nanostructures considered as the size of a coherently diffracting domain may or may not be the same as the individual particle's size. XRD peak broadening was observed to be strikingly obvious in case of GSH-capped CuO nanoparticles (Fig. 3b) which might have occurred as a result of deformation, crystallite size, microstrains and instrumental broadening [26]. Dislocation density was found inversely proportional to the crystallite size derived by Sherrer's equation with increased dislocation density observed in case of GSH-CuO with smaller mean crystallite size. This suggests that GSH-CuO nanostructure might be more defective probably due to subjection to further surface modification. SEM analyses of both types of nanostructures were in correspondence to the crystallite size obtained through XRD with decreased size identified in case of GSH capped CuO nanospheres (Fig. 4).

4.4. Stability analysis

The stability of nanoparticles in the presence of diverse compositions is of immense importance because it enables their applicability in multi-ranged biological applications. Therefore, biologically synthesized CuO nanostructures in the current study were analyzed for their stability in the presence of certain distinct compounds selected on the

Table 3
Comparison of kinetic parameters of CuO and GSH-CuO nanospheres with other peroxidase mimicking nanostructures with H_2O_2 as oxidant.

No.	POx mimicking entity	Substrate	Michaelis Menten constant K_m (mM)	References
1.	`CS-GO NPs	TMB	0.033	[34]
2.	BSA-Au NPs	TMB	0.00253	[35]
3.	Pt NCs	TMB	0.096	[36]
4.	Cu NPs	TMB	0.648	[37]
5.	Ag/rGO	TMB	0.850	[38]
6.	Zn-CuO	TMB	0.01	[19]
7.	CuO NPs	TMB	1.600	this work
8.	GSH-CuO NPs	TMB	0.32	this work

CS-Graphene: Chitosan stabilized graphene oxide nanoparticles, BSA-Au: Bovine serum albumin stabilized Gold nanoparticles, HCNTs: Helical-Carbon nanotubes.

basis of their biomedical implications. Among various tested compounds, CuO nanospheres, both uncapped and GSH-capped were found significantly stable in the presence of Catechin hydrate, $HgCl_2$, Phenol and Lead nitrate after 24 h incubation period (Fig. 5). All of these compounds have profound therapeutic and biomedical importance [31–33]. Thus, the investigated compatibility of synthesized nanoparticles increases their likelihood to be used in bio-applications executed in the presence of above mentioned compounds.

4.5. Kinetics studies of CuO/GSH-CuO nanospheres

At present, numerous researches have been performed in determining the nanozymatic potential of metal nanoparticles however, majority of the work involves chemically/physically synthesized nanostructures with almost no reference to biologically synthesized nanoparticles serving as biosensors. Therefore, present research was focused on determining the peroxidase like activity of nanospheres synthesized from aqueous extract of *Berberis lycium* with an aim to introduce cost-effective, non-toxic and biocompatible nanozymes. In order to compare the catalytic affinity of CuO and GSH-CuO nanospheres with that of standard peroxidase enzyme, firstly the kinetic parameters of HRP were studied with H_2O_2 and TMB as the substrates. After HRP, same reaction was carried out under optimized conditions to analyze the intrinsic peroxidase activity of prepared NPs. Evaluation of overall catalytic efficacy of phyto-synthesized nanospheres demonstrated moderate catalytic efficiency in both cases i.e. CuO and GSH-CuO nanospheres compared to the native HRP. However, GSH-CuO nanospheres showed better results in contrast to uncapped types. Table 3 compares the catalytic affinities of synthesized nanospheres with some of the previously reported enzyme mimicking materials [34–38]. Increased affinity for TMB exhibited by GSH-CuO NPs compared to uncapped CuO nanospheres might have occurred because their smaller size might have provided more surface area and hence increased number of active catalytic sites to the substrate.

None of the compounds tested as potential enhancers were observed to support the enzyme mimicking activity of prepared nanozymes although surprisingly, TMB oxidation rate in case of HRP was found increased in the presence of Lead nitrate. Previously, metal cofactors such as Ca^{2+} and Fe^{2+} in heme group have been recognized as boosters of refolding yield as well as catalytic activity of HRP [39]. However, the exact role of Lead nitrate in the functioning and stability of HRP is yet to be studied.

4.6. Mechanism behind POx activity of CuO/GSH-CuO nanospheres

The possible mechanism that can be suggested for peroxidase mimicking activity of synthesized nanoparticles is that TMB was adsorbed on to the surface of nanospheres through π-π stacking interaction between free electrons and conduction band electrons of metallic nanoparticles [34]. TMB then donated its lone electron pair of amino group to nanoparticles thereby converting itself to oxidized blue complex with maximum absorbance at 652 nm. Meanwhile, the electrons donated to nanospheres by TMB increased the electron density and mobility which compelled CuO/GSH-CuO nanostructures to transfer electron to H_2O_2 thus reducing H_2O_2 into water. Relatively, better redox activity was displayed by GSH-CuO probably because of the quantum size effect exhibited by smaller crystalline size of capped nanospheres, thereby speeding up the process of electron transfer from TMB to H_2O_2 [40]. Also, it can be suggested for better activity of GSH-CuO that TMB was easily adsorbed on its large surface area due to increased density of catalytically active sites. Moreover, the reducing ability of glutathione might have played an influential role in enhancing catalytic activity of GSH-CuO nanospheres.

5. Conclusion

In conclusion, glutathione stabilized and non-functionalized CuO nanospheres were found stable in the presence of certain bio-medically significant compounds which broadens their spectra of applicability. CuO nanospheres with wide-ranged stability can emerge as potential remediators of environmental toxicants. Although synthesized nanoparticles depicted marginal catalytic efficiency compared to previously reported POx mimicking nanostructures [41,42], the use of biological extract as reducing agent and Glutathione as capping agent for nanozymes' synthesis is the striking feature of current research work which made the whole process more cost effective, time-saving, non-toxic and environment friendly. Hence, there is a plausible chance that further manipulation and optimization of synthesizing parameters and reaction conditions may give rise to efficient and stable phyto-synthesized GSH-CuO nanozymes which may serve as better alternatives to chemically/physically formulated colorimetric Nano-biosensors.

Funding source

University research fund allocated by the Government of Pakistan is the basic funding source for accomplishment of this research project.

Declarations of interests

None.

Appendix A. Supplementary data

Supplementary material related to this article can be found, in the online version, at doi:https://doi.org/10.1016/j.colsurfb.2019.02.048.

References

[1] V.V. Makarov, A.J. Love, O.V. Sinitsyna, S.S. Makarova, I.V. Yaminsky, M.E. Taliansky, N.O. Kalinina, "Green" nanotechnologies: synthesis of metal nanoparticles using plants, Acta Nat. 6 (1) (2014) 20 PMCID: PMC399946.
[2] H.R. Naika, K. Lingaraju, K. Manjunath, D. Kumar, G. Nagaraju, D. Suresh, H. Nagabhushana, Green synthesis of CuO nanoparticles using Gloriosasuperba L. extract and their antibacterial activity, J. Taibah Univ. Sci. 9 (1) (2015) 7–12, https://doi.org/10.1016/j.jtusci.2014.04.006.
[3] D. Rehana, D. Mahendiran, R.S. Kumar, A.K. Rahiman, Evaluation of antioxidant and anticancer activity of copper oxide nanoparticles synthesized using medicinally important plant extracts, Biomed. Pharmacother. 89 (2017) 1067–1077, https://doi.org/10.1016/j.biopha.2017.02.101.
[4] A.B. Rezaie, M. Montazer, M.M. Rad, Photo and bio catalytic activities along with UV protection properties on polyester fabric through green in-situ synthesis of cauliflower-like CuO nanoparticles, J. Photochem. Photobiol. B: Biol. 176 (2017) 100–111, https://doi.org/10.1016/j.jphotobiol.2017.09.021.
[5] M. Bordbar, N. Negahdar, M. Nasrollahzadeh, Melissa Officinalis L. leaf extract assisted green synthesis of CuO/ZnO nanocomposite for the reduction of 4-nitrophenol and rhodamine B, Sep. Purif. Technol. 191 (2018) 295–300, https://doi.org/10.1016/j.seppur.2017.09.044.
[6] P.C. Nethravathi, M.P. Kumar, D. Suresh, K. Lingaraju, H. Rajanaika, H. Nagabhushana, S.C. Sharma, Tinospora cordifolia mediated facile green synthesis of cupric oxide nanoparticles and their photocatalytic, antioxidant and

antibacterial properties, Mater. Sci. Semicond. Process. 33 (2015) 81–88, https://doi.org/10.1016/j.mssp.2015.01.034.
[7] Z. Issaabadi, M. Nasrollahzadeh, S.M. Sajadi, Green synthesis of the copper nanoparticles supported on bentonite and investigation of its catalytic activity, J. Clean. Prod. 142 (2017) 3584–3591, https://doi.org/10.1016/j.jclepro.2016.10.109.
[8] Y. Tauran, A. Brioude, A.W. Coleman, M. Rhimi, B. Kim, Molecular recognition by gold, silver and copper nanoparticles, World J. Biol. Chem. 4 (3) (2013) 35–63, https://doi.org/10.4331/wjbc.v4.i3.35.
[9] W. Li, H. Zhang, J. Zhang, Y. Fu, Synthesis and sensing application of glutathione-capped platinum nanoparticles, Anal. Methods 7 (11) (2015) 4464–4471, https://doi.org/10.1039/C5AY00365B.
[10] P. Sharma, A.B. Jha, R.S. Dubey, M. Pessarakli, Reactive oxygen species, oxidative damage, and antioxidative defense mechanism in plants under stressful conditions, J. Bot. 2012 (2012), https://doi.org/10.1155/2012/217037.
[11] H. Wei, E. Wang, Nanomaterials with enzyme-like characteristics (nanozymes): next-generation artificial enzymes, Chem. Soc. Rev. 42 (14) (2013) 6060–6093, https://doi.org/10.1039/c3cs35486e.
[12] L. Han, C. Li, T. Zhang, Q. Lang, A. Liu, Au@Ag heterogeneous nanorods as nanozyme interfaces with peroxidase-like activity and their application for one-pot analysis of glucose at nearly neutral pH, ACS Appl. Mater. Interfaces 7 (26) (2015) 14463–14470, https://doi.org/10.1021/acsami.5b03591.
[13] A.J. Saleh Ahammad, Hydrogen peroxide biosensors based on horseradish peroxidase and hemoglobin, J. Biosens. Bioelectron. 9 (2013) 2, https://doi.org/10.4172/2155-6210.S9-001.
[14] Y. Jv, B. Li, R. Cao, Positively-charged gold nanoparticles as peroxidase mimic and their application in hydrogen peroxide and glucose detection, Chem. Commun. 46 (42) (2010) 8017–8019, https://doi.org/10.1039/C0CC02698K.
[15] C.M. Maroneze, G.P. Dos Santos, V.B. de Moraes, L.P. da Costa, L.T. Kubota, Multifunctional catalytic platform for peroxidase mimicking, enzyme immobilization and bio sensing, Biosens. Bioelectron. 77 (2016) 746–751, https://doi.org/10.1016/j.bios.2015.10.042.
[16] J. Zhao, W. Dong, X. Zhang, H. Chai, Y. Huang, FeNPs@Co3O4 hollow nanocages hybrids as effective peroxidase mimics for glucose bio sensing, Sens. Actuators B: Chem. 263 (2018) 575–584, https://doi.org/10.1016/j.snb.2018.02.151.
[17] N.S. Vallabani, A.S. Karakoti, S. Singh, ATP-mediated intrinsic peroxidase-like activity of Fe3O4-based nanozyme: one step detection of blood glucose at physiological pH, Colloids Surf. B: Biointerfaces 153 (2017) 52–60, https://doi.org/10.1016/j.colsurfb.2017.02.004.
[18] Y. Liu, Y. Zheng, D. Ding, R. Guo, Switching peroxidase-mimic activity of protein stabilized platinum nanozymes by sulfide ions: substrate dependence, mechanism, and detection, Langmuir 33 (48) (2017) 13811–13820, https://doi.org/10.1021/acs.langmuir.7b03430.
[19] T.G. Choleva, V.A. Gatselou, G.Z. Tsogas, D.L. Giokas, Intrinsic peroxidase-like activity of rhodium nanoparticles, and their application to the colorimetric determination of hydrogen peroxide and glucose, Microchim. Acta 185 (1) (2018) 22, https://doi.org/10.1007/s00604-017-2582-8.
[20] H. Ali, S. Uddin, S. Jalal, Chemistry and biological activities of Berberis lycium Royle, J. Biol. Act. Prod. Nat. 5 (5) (2015) 295–312, https://doi.org/10.1080/22311866.2015.1073627.
[21] N. ul Ain, N. Safdar, A. Yasmin, Antimicrobial investigations from crude and peptide extracts of Glycine max Linn. Merr varieties, Arab. J. Sci. Eng. 42 (1) (2017) 105–113, https://doi.org/10.1007/s13369-016-2248-6.
[22] R. Sankar, P. Manikandan, V. Malarvizhi, T. Fathima, K.S. Shivashangari, V. Ravikumar, Green synthesis of colloidal copper oxide nanoparticles using Carica papaya and its application in photocatalytic dye degradation, Spectrochim. Acta A: Mol. Biomol. Spectrosc. 121 (2014) 746–750, https://doi.org/10.1016/j.saa.2013.12.020.
[23] G.H. Wang, J. Hilgert, F.H. Richter, F. Wang, H.J. Bongard, B. Spliethoff, C. Weidenthaler, F. Schüth, Platinum–cobalt bimetallic nanoparticles in hollow carbon nanospheres for hydrogenolysis of 5-hydroxymethylfurfural, Nat. Mater. 13 (3) (2014) 293–300, https://doi.org/10.1038/nmat3872.
[24] W. Shi, Q. Wang, Y. Long, Z. Cheng, S. Chen, H. Zheng, Y. Huang, Carbon nanodots as peroxidase mimetics and their applications to glucose detection, Chem. Commun. 47 (23) (2011) 6695–6697, https://doi.org/10.1039/C1CC11943E.
[25] A.P. Nagvenkar, A. Gedanken, Cu0.89Zn0.11O, a new peroxidase-mimicking nanozyme with high sensitivity for glucose and antioxidant detection, ACS Appl. Mater. Interfaces 8 (34) (2016) 22301–22308, https://doi.org/10.1021/acsami.6b05354.
[26] P. Bindu, S. Thomas, Estimation of lattice strain in ZnO nanoparticles: X-ray peak profile analysis, J. Theor. Appl. Phys. 8 (4) (2014) 123–134, https://doi.org/10.1007/s40094-014-0141-9.
[27] F. Duman, I. Ocsoy, F.O. Kup, Chamomile flower extract-directed CuO nanoparticle formation for its antioxidant and DNA cleavage properties, Mater. Sci. Eng. C 60 (2016) 333–338, https://doi.org/10.1016/j.msec.2015.11.052.
[28] N. Zayyoun, L. Bahmad, L. Laânab, B. Jaber, The effect of pH on the synthesis of stable Cu_2O/CuO nanoparticles by sol–gel method in a glycolic medium, Appl. Phys. A 122 (5) (2016) 488, https://doi.org/10.1007/s00339-016-0024-9.
[29] P.K. Singh, P. Kumar, M. Hussain, A.K. Das, G.C. Nayak, Synthesis and characterization of CuO nanoparticles using strong base electrolyte through electrochemical discharge process, Bull. Mater. Sci. 39 (2) (2016) 469–478, https://doi.org/10.1007/s12034-016-1159-1.
[30] S. Krishnan, A.S.M.A. Haseeb, M.R. Johan, Synthesis and growth kinetics of spindly CuO nanocrystals via pulsed wire explosion in liquid medium, J. Nanopart. Res. 15 (1) (2013) 1410, https://doi.org/10.1007/s11051-012-1410-7.
[31] A. Smith, B. Giunta, P.C. Bickford, M. Fountain, J. Tan, R.D. Shytle, Nanolipidic particles improve the bioavailability and α-secretase inducing ability of epigallocatechin-3-gallate (EGCG) for the treatment of Alzheimer's disease, Int. J. Pharm. 389 (1-2) (2010) 207–212, https://doi.org/10.1016/j.ijpharm.2010.01.012.
[32] M.A. Ansari, A. Anurag, Z. Fatima, S. Hameed, Natural phenolic compounds: a potential antifungal agent, Microb (2013) 189–195, https://doi.org/10.1155/2014/895193.
[33] M.M. Naik, S.K. Dubey, Lead resistant bacteria: lead resistance mechanisms, their applications in lead bioremediation and biomonitoring, Ecotoxicol. Environ. Saf. 98 (2013) 1–7, https://doi.org/10.1016/j.ecoenv.2013.09.039.
[34] G.L. Wang, X. Xu, X. Wu, G. Cao, Y. Dong, Z. Li, Visible-light-stimulated enzyme like activity of graphene oxide and its application for facile glucose sensing, J. Phys. Chem. C 118 (48) (2014) 28109–28117, https://doi.org/10.1021/jp5088543.
[35] X.X. Wang, Q. Wu, Z. Shan, Q.M. Huang, BSA-stabilized Au clusters as peroxidase mimetics for use in xanthine detection, Biosens. Bioelectron. 26 (8) (2011) 3614–3619, https://doi.org/10.1016/j.bios.2011.02.014.
[36] L. Jin, Z. Meng, Y. Zhang, S. Cai, Z. Zhang, C. Li, L. Shang, Y. Shen, Ultrasmall Pt nanoclusters as robust peroxidase mimics for colorimetric detection of glucose in human serum, ACS Appl. Mater. Interfaces 9 (11) (2017) 10027–10033, https://doi.org/10.1021/acsami.7b01616.
[37] L. Hu, Y. Yuan, L. Zhang, J. Zhao, S. Majeed, G. Xu, Copper nanoclusters as peroxidase mimetics and their applications to H_2O_2 and glucose detection, Anal. Chim. Acta 762 (2013) 83–86, https://doi.org/10.1016/j.aca.2012.11.056.
[38] G. Darabdhara, B. Sharma, M.R. Das, R. Boukherroub, S. Szunerits, Cu-Ag bimetallic nanoparticles on reduced graphene oxide nanosheets as peroxidase mimic for glucose and ascorbic acid detection, Sens. Actuators B: Chem. 238 (2017) 842–851, https://doi.org/10.1016/j.snb.2016.07.106.
[39] S.W. Bae, D. Eom, N.L. Mai, Y.M. Koo, Refolding of horseradish peroxidase is enhanced in presence of metal cofactors and ionic liquids, Biotechnol. J. 11 (4) (2016) 464–472, https://doi.org/10.1002/biot.201500142.
[40] Z. Gao, M. Xu, L. Hou, G. Chen, D. Tang, Irregular-shaped platinum nanoparticles as peroxidase mimics for highly efficient colorimetric immunoassay, Anal. Chim. Acta 776 (2013) 79–86, https://doi.org/10.1016/j.aca.2013.03.034.
[41] J. Mu, J. Li, X. Zhao, E.C. Yang, X.J. Zhao, Cobalt-doped graphitic carbon nitride with enhanced peroxidase-like activity for wastewater treatment, RSC Adv. 6 (42) (2016) 35568–35576, https://doi.org/10.1039/C6RA02911F.
[42] W. Chen, J. Chen, A.L. Liu, L.M. Wang, G.W. Li, X.H. Lin, Peroxidase-like activity of cupric oxide nanoparticle, ChemCatChem 3 (7) (2011) 1151–1154, https://doi.org/10.1002/cctc.201100064.